Available online at www.sciencedirect.com
SCIENCE DIRECT®
Journal of Sound and Vibration 284 (2005) 597–612
JOURNAL OF SOUND AND VIBRATION
www.elsevier.com/locate/jsvi

Effect of piezoelectric damping layers on the dynamic stability of plate under a thrust

Hui-Won Kim, Ji-Hwan Kim*

School of Mechanical and Aerospace Engineering, College of Engineering, Seoul National University, San 56-1, Shinrim-dong, Kwanak-ku, Seoul 151-742, Republic of Korea

Received 7 November 2003; accepted 25 June 2004
Available online 20 December 2004

Abstract

In this study, the dynamic stability of plate with the active-damping layer under a thrust is investigated. The structure is actively damped by piezoelectric layers, and adopted a control algorithm for vibration suppression. Thin piezoelectric layers are assumed to be embedded on the top and the bottom surfaces of the structure. The top and the bottom layers are taken as the actuator and the sensor, respectively.

The structure model is based on the first-order shear deformation plate theory, and the finite element method is applied in the numerical analysis. In addition, the method of multiple scales is adopted to analyze the parametrically excited system. This analysis is specifically focused on the mutual interaction of the thrust and the piezoelectric active-damping layer for the vibration suppression. In this paper, the effects of the active-damping layer with piezoelectric sensors/actuators are discussed in detail.

1. Introduction

Adaptive design, namely active sensing and control of structures, has been a topic that has drawn great attention among researches and on which significant amount of work has already

*Corresponding author. Tel.: +82 2880 7383; fax: +82 2887 2662.
E-mail address: jwhkim@snu.ac.kr (J.-H. Kim).

0022-460X/$ - see front matter © 2004 Elsevier Ltd. All rights reserved.
doi:10.1016/j.jsv.2004.06.045

Nomenclature

u,v,w	displacements
B	strain–displacement matrix
σ_i, ε_i	stress and strain components
$\{\varepsilon_m\}$	inplane strain vector
E_i	electric field components
D_i	electric displacement components
Q_{ij}	plane-stress reduced elastic constants
e_{ij}	piezoelectric constants
Ξ_{ij}	permittivity coefficients
T,U	kinetic energy and potential energy
W_c	work of the conservative part of thrust P
δW_{nc}	virtual work of the non-conservative part of thrust P
M	mass matrix
K	stiffness matrix by the strain energy
K_g	stiffness matrix by the external load
$\bar{\delta}(x)$	Dirac delta function
G_c	gain of the current amplifier
G_i	gain to provide feedback control
G	control gain
λ	aspect ratio of plate (length per width)
γ	thickness ratio of plate
$\bar{m}$	mass per unit area
D	bending rigidity of plate
ω	natural frequency
Ω	non-dimensional frequency
Q	non-dimensional thrust
Ω_{dr}	driving frequency
α	static load factor
β	pulsating load factor
μ	damping coefficient

been done. Furthermore, many researchers have studied the smart structures using various materials such as shape memory alloys, piezoelectric materials, electrostrictive materials, magneto-strictive materials and electro-rheological fluids. Among these, piezoelectric materials have been most widely used due to its advantages such as the fact that it is inexpensive, light weighted, and can be easily shaped and bonded to surfaces or embedded into structures. The main features of piezoelectric materials are the direct and converse piezoelectric effects. That is, the materials generate an electric charge during a mechanical deformation, while mechanical stress or strain is produced only by an applied electric field. By applying these properties of the material, smart structures can be tailored to act as distributed sensors/actuators in the active control of dynamic systems.

Lam et al. [1] and Liu et al. [2] actively controlled the dynamic response of a composite plate with distributed piezoelectric sensors/actuators by using a simple negative velocity feedback control algorithm. Saravanan et al. [3] studied active damping in a composite cylindrical shell with collocated piezoelectric sensors/actuators for the effects of locations, percentage lengths, and skew angles. Balamurugan and Narayanan [4] developed a new piezo-laminated quadrilateral composite plate/shell finite element, and analyzed vibration control performance of the structures. They considered control effectiveness of several control strategies such as direct proportional feedback, constant-gain negative velocity feedback and Lyapunov feedback. Tzou et al. [5,6] investigated the spatial sensing and actuation effectiveness of shell transducer patches, and studied the contributions of membrane and bending control effects. St-Amant and Cheng [7] conducted simulations and experiments on active vibration control of a plate with integrated piezoceramics and various control algorithms. Niezrecki and Cudney [8] created and verified a simply supported cylinder with PZT actuator experimentally. Hwang and Park [9] made a finite element formulation for vibration control of a laminated plate with piezoelectric sensors/actuators. Reddy [10] arranged various formulations for laminated composite

plates with integrated sensors/actuators under the simultaneous mechanical and electrical loadings.

Space structures need to transfer orbits or move to desired positions, and the structures may undergo dynamic instability such as flutter, divergence, and parametric resonance due to a thrust. Higuchi and Dowell [11,12] studied the dynamic stability of a completely free panel under a follower force. This is an example of space structures subjected to a rocket thrust. Nayfeh and Mook [13] developed the method of multiple scales to analyze the parametrically excited systems. Choo and Kim [14] analyzed the dynamic instability of rectangular plates with four-free edges under a constant and pulsating follower force. They investigated the instability regions for composite plates in detail. Kim and Kim [15] studied the parametric instability of a laminated viscoelastic beam under a periodic loading, and summarized the stabilizing effect of viscoelasticity of the material. Langthjem and Sugiyama [16] offered a survey of simple structural elements subjected to a follower force. Svensson [17] investigated the stability properties of a periodically loaded nonlinear dynamic system, and specially gave particular attention to damping effects. Xin-Mai Yang and Ya-Peng Shen [18] analyzed the dynamic instability region of a laminated cylindrical shells subjected to a parametric excitation. Lien-Wen Chen et al. [19] evaluated the effect of feedback control gain on the dynamic stability of a composite beam.

To control the dynamic behavior of system under the dynamic loading, it is desirable to create damping without increasing the structural rigidity of the material. Thus, there have been many research works on actively damped system with the exception of smart structures under a follower force. In this paper, it is focused on the structures with piezoelectric active-damping layer under a thrust. In other words, the mutual interaction of dynamic stability of structures and piezoelectric active-damping layers for the vibration suppression is investigated.

2. Formulation

Fig. 1 shows the schematic diagram of the piezo-laminated rectangular plate and feedback control algorithm under a thrust.

2.1. Constitutive equations and piezoelectric coupling

Assuming linear piezoelectric coupling between the elastic field and the electric field in the kth layer, the direct and the converse piezoelectric equations for the first-order shear deformation theory(FSDT) are [10]

$$\begin{Bmatrix} D_x \\ D_y \\ D_z \end{Bmatrix}_k = \begin{bmatrix} 0 & 0 & 0 \\ 0 & 0 & 0 \\ \bar{e}_{31} & \bar{e}_{32} & \bar{e}_{36} \end{bmatrix}_k \begin{Bmatrix} \varepsilon_x \\ \varepsilon_y \\ \gamma_{xy} \end{Bmatrix} + \begin{bmatrix} \bar{e}_{14} & \bar{e}_{15} \\ \bar{e}_{24} & \bar{e}_{25} \\ 0 & 0 \end{bmatrix}_k \begin{Bmatrix} \gamma_{yz} \\ \gamma_{xz} \end{Bmatrix} + \begin{bmatrix} \bar{\Xi}_{11} & \bar{\Xi}_{12} & 0 \\ \bar{\Xi}_{12} & \bar{\Xi}_{22} & 0 \\ 0 & 0 & \bar{\Xi}_{33} \end{bmatrix}_k \begin{Bmatrix} E_x \\ E_y \\ E_z \end{Bmatrix}_k, \quad (1)$$

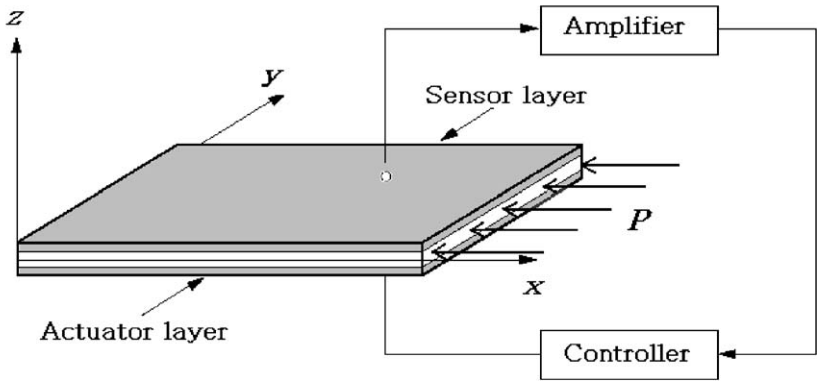

Fig. 1. Piezo-laminated plate and feedback control algorithm under a thrust P.

$$\begin{Bmatrix} \sigma_x \\ \sigma_y \\ \sigma_{xy} \end{Bmatrix}_k = \begin{bmatrix} \bar{Q}_{11} & \bar{Q}_{12} & \bar{Q}_{16} \\ \bar{Q}_{12} & \bar{Q}_{22} & \bar{Q}_{26} \\ \bar{Q}_{16} & \bar{Q}_{26} & \bar{Q}_{66} \end{bmatrix}_k \begin{Bmatrix} \varepsilon_x \\ \varepsilon_y \\ \gamma_{xy} \end{Bmatrix} - \begin{bmatrix} 0 & 0 & \bar{e}_{31} \\ 0 & 0 & \bar{e}_{32} \\ 0 & 0 & \bar{e}_{36} \end{bmatrix}_k \begin{Bmatrix} E_x \\ E_y \\ E_z \end{Bmatrix}_k,$$

$$\begin{Bmatrix} \sigma_{yz} \\ \sigma_{xz} \end{Bmatrix}_k = \begin{bmatrix} \bar{Q}_{44} & \bar{Q}_{45} \\ \bar{Q}_{45} & \bar{Q}_{55} \end{bmatrix}_k \begin{Bmatrix} \gamma_{yz} \\ \gamma_{xz} \end{Bmatrix} + \begin{bmatrix} \bar{e}_{14} & \bar{e}_{24} & 0 \\ \bar{e}_{15} & \bar{e}_{25} & 0 \end{bmatrix}_k \begin{Bmatrix} E_x \\ E_y \\ E_z \end{Bmatrix}_k, \tag{2}$$

where the upper-bar means the transformed quantity to the xyz coordinate.

2.2. Displacement field for FSDT

The displacement field is based on the FSDT, that is, the displacements u, v and w at a point (x, y, z) are expressed as functions of mid-plane displacements u_0, v_0, w_0 and independent rotations ϕ_x and ϕ_y of the normals in the xz and yz planes, respectively.

$$\begin{aligned} u(x, y, z, t) &= u_0(x, y, t) + z\phi_x(x, y, t), \\ v(x, y, z, t) &= v_0(x, y, t) + z\phi_y(x, y, t), \\ w(x, y, z, t) &= w_0(x, y, t). \end{aligned} \tag{3}$$

In this study, each respective five degrees of freedom (u_0, v_0, w_0, ϕ_x, ϕ_y) is interpolated over an element as 16-node Lagrangian element.

2.3. Equations of motion

Equations of motion of the piezo-laminated plate can be derived by the extended Hamilton's principle

$$\delta \int_{t_1}^{t_2} (T - U + W_c)\, \mathrm{d}t + \int_{t_1}^{t_2} \delta W_{\mathrm{nc}}\, \mathrm{d}t = 0, \tag{4}$$

where

$$T = \frac{1}{2}\rho \int_V (\dot{u}^2 + \dot{v}^2 + \dot{w}^2)\,\mathrm{d}V,$$

$$U = \frac{1}{2}\int_V \{\varepsilon\}^{\mathrm{T}}\{\sigma\}\,\mathrm{d}V = \frac{1}{2}\int_V \{\varepsilon\}^{\mathrm{T}}[\bar{Q}]\{E\}\,\mathrm{d}V - \frac{1}{2}\int_V \{\varepsilon\}^{\mathrm{T}}[\bar{e}]^{\mathrm{T}}\{E\}\,\mathrm{d}V,$$

$$W_c = \frac{1}{2}\int\int_A P(t)\frac{x}{a}\left(\frac{\partial w}{\partial x}\right)^2 \mathrm{d}A,$$

$$\delta W_{\mathrm{nc}} = -\int\int_A P(t)\frac{\partial w}{\partial x}\bar{\delta}(x-a)\delta w\,\mathrm{d}A, \tag{5}$$

where $P(t)$ and a are the follower force and the length of the plate to the x direction, respectively.

Actuator layer with thickness h_A is assumed to be applied with a voltage V^e only in the thickness direction, the electric field vector $\{E\}$ can be expressed as [1]

$$\{E\} = \begin{bmatrix}0 & 0 & 1/h_A\end{bmatrix}^{\mathrm{T}} V^e = [B_v]V^e. \tag{6}$$

The finite element method is applied, after which the matrix equation of motion can be obtained as follows [1,14,15]:

$$[M]\{\ddot{d}\} + [K]\{d\} - P(t)[K_g]\{d\} = [K_{\mathrm{av}}]V^e, \tag{7}$$

where the displacement vector and $[K_{\mathrm{av}}]$ are defined as follows:

$$\{d\} = [u_0 \quad v_0 \quad w_0 \quad \phi_x \quad \phi_y]^{\mathrm{T}}, \tag{8}$$

$$[K_{\mathrm{av}}] = \int_V [B]^{\mathrm{T}}[\bar{e}]^{\mathrm{T}}[B_v]\,\mathrm{d}V. \tag{9}$$

2.4. Sensor equation and active control

Total charge developed on the sensor surface is the spatial summation of all the point charges on the sensor layer. In this study, it is assumed that the whole piezoelectric lamina serves as the effective surface electrode.

Then, the total charge $q(t)$ can be written as follows:

$$q(t) = \sum_{j=1}^{Ns}\frac{1}{2}\left[\int_{S_j(z=z_k)} D_z\,\mathrm{d}S + \int_{S_j(z=z_{k+1})} D_z\,\mathrm{d}S\right], \tag{10}$$

where N_s denotes the number of elements, S_j is the surface of the jth element, and

$$D_z = \bar{e}_{31}\varepsilon_x + \bar{e}_{32}\varepsilon_y + \bar{e}_{36}\gamma_{xy} = [\bar{e}_3]\{\varepsilon_m\}. \tag{11}$$

Thus, the current $i(t)$ on the surface of a sensor is expressed as

$$i(t) = \frac{\mathrm{d}q(t)}{\mathrm{d}t}. \tag{12}$$

Piezoelectric sensors are assumed to be used as strain rate sensors, then the current can be converted into voltage output V_s as

$$V_s(t) = G_c i(t) = G_c \frac{\mathrm{d}q(t)}{\mathrm{d}t}, \tag{13}$$

where G_c is the gain of the current amplifier, which transforms the sensor current to voltage.

The distributed sensor generates a voltage when the structure is oscillating, and this signal is fed back into the distributed actuator. Using a constant gain control algorithm as in Ref. [1], the actuating voltage can be expressed as

$$V^e = G_i V_s = G_i G_c \frac{\mathrm{d}q}{\mathrm{d}t}, \tag{14}$$

where G_i is the gain to provide feedback control.

Therefore, the actuating voltages V^e can be written as [1]

$$V^e = [G][K_{\mathrm{sv}}]\{\dot{d}\}, \tag{15}$$

where

$$G = G_i G_c,$$

$$[K_{\mathrm{sv}}] = \sum_{j=1}^{N_s} \frac{1}{2} \left[\int_{S_j(z=z_k)} [\bar{e}_3][B]\,\mathrm{d}S + \int_{S_j(z=z_{k+1})} [\bar{e}_3][B]\,\mathrm{d}S \right]. \tag{16}$$

Now, Eq. (7) can be rewritten as

$$[M]\{\ddot{d}\} - [K_{\mathrm{av}}][G][K_{\mathrm{sv}}]\{\dot{d}\} + ([K] - P(t)[K_g])\{d\} = \{0\}. \tag{17}$$

3. Dynamic stability analysis

If a structure is subjected to a constant follower force, it may undergo divergence or flutter instability. Furthermore, small damping sometimes destabilizes a flexible system, requiring the need to check the dynamic stability characteristics of the structure using the eigenvalue analysis.

For a parametrically excited system, let

$$P(t) = P_0 + P_1 \cos\ \Omega_{\mathrm{dr}} t. \tag{18}$$

Then, Eq. (17) becomes

$$[M]\{\ddot{d}\} - [K_{\mathrm{av}}][G][K_{\mathrm{sv}}]\{\dot{d}\} + ([K] - P_0[K_g])\{d\} - P_1 \cos\ \Omega_{\mathrm{dr}} t[K_g]\{d\} = \{0\}. \tag{19}$$

Introducing G^* as standard magnitude of control gain, and P_{cr} as the critical value of the constant follower force,

$$[M]\{\ddot{d}\} - \mu[K_{\mathrm{av}}][G^*][K_{\mathrm{sv}}]\{\dot{d}\} + ([K] - \alpha P_{\mathrm{cr}}[K_g])\{d\} - \beta P_{\mathrm{cr}} \cos\ \Omega_{\mathrm{dr}} t[K_g]\{d\} = \{0\}, \tag{20}$$

where μ, α and β means G/G^*, P_0/P_{cr} and P_1/P_{cr}, respectively.

By using modal transformation, we can transform $[M]$ and $[K]$ into diagonal matrices. Generally, three translation and three rotation modes are observed for a plate structure. We assume that such rigid-body modes can be controlled by proper method [14].

Let $[\Phi]$ and $[\Psi]$ be the $n \times (n-p)$ normalized right and left modal matrices, where p is the number of rigid body modes that is assumed to be controlled. Introducing the linear transformation $\{d\} = [\Phi]\{\eta\}$ and pre-multiplying $[\Psi]^{\mathrm{T}}$ on each term, the equations of motion can be obtained as [14]

$$[I]\{\ddot{\eta}\} - \mu[C]\{\dot{\eta}\} + [\Lambda]\{\eta\} - \beta \cos \Omega_{\mathrm{dr}} t[R]\{\eta\} = 0, \tag{21}$$

where $[\Psi]^{\mathrm{T}}[M][\Phi] = [I]$, $[\Psi]^{\mathrm{T}}[K][\Phi] = [\Lambda]$, $[\Psi]^{\mathrm{T}}[K_g][\Phi] = [R]$.

In component form,

$$\ddot{\eta}_j + \mu \sum_{m=1}^{n} C_{jm}\dot{\eta}_m + \omega_j^2 \eta_j + 2\varepsilon \cos \Omega_{\mathrm{dr}} t \sum_{m=1}^{n} R_{jm}\eta_m = 0, \tag{22}$$

where

$$j = 1, 2, 3, \ldots, n-p, \quad \varepsilon = -\beta/2.$$

Using the method of multiple scales as in Ref. [13] by the first-order expansion of μ and ε,

$$\eta_j(T_0, T_1, T_2) = \eta_{j0}(T_0, T_1, T_2) + \mu\eta_{j1}(T_0, T_1, T_2) + \varepsilon\eta_{j2}(T_0, T_1, T_2), \tag{23}$$

where $T_0 = t$ and $T_1 = \mu t$, $T_2 = \varepsilon t$ are the so-called fast-scale and slow scales, respectively, and note that ε used in Eq. (23) does not mean the strain used in Section 2.3.

Substituting Eq. (23) into Eq. (22),

$$D_0^2\eta_{j0} + \omega_j^2\eta_{j0} = 0, \tag{24}$$

$$D_0^2\eta_{j1} + \omega_j^2\eta_{j1} = -2D_0D_1\eta_{j0} - \sum_{m=1}^{n} C_{jm}D_0\eta_{m0}, \tag{25}$$

$$D_0^2\eta_{j2} + \omega_j^2\eta_{j2} = -2D_0D_2\eta_{j0} - [\exp(\mathrm{i}\Omega_{\mathrm{dr}}T_0) + \exp(-\mathrm{i}\Omega_{\mathrm{dr}}T_0)] \sum_{m=1}^{n} R_{jm}\eta_{m0}, \tag{26}$$

where $D_k = \partial/\partial T_k$, $j = 1, 2, 3, \ldots, n-p$.

General solution of Eq. (24) is,

$$\eta_{j0} = A_j(T_1, T_2)\exp(\mathrm{i}\omega_j T_0) + \text{c.c.} \tag{27}$$

where c.c. represents the complex conjugate of the preceding terms.

Inserting Eq. (27) into Eqs. (25) and (26), equations with secular terms that are unbounded with time can be derived. Complex functions A_j are determined by eliminating the terms from Eqs. (25) and (26) which produce the troublesome secular and small-divisor terms in η_{j1}, η_{j2}. In this way, two types of transition curves that separate stable solutions from unstable ones in the ε–Ω_{dr} plane can be defined [15].

For $\Omega_{dr}=\omega_p+\omega_q$, the sum-type combination resonance as [14]

$$\Omega_{dr}=\omega_p+\omega_q\pm\varepsilon\sqrt{\frac{R_{pq}R_{qp}}{\omega_p\omega_q}-\left(\frac{\mu C_{ii}}{\varepsilon}\right)^2}. \tag{28}$$

For $\Omega_{dr}=\omega_q-\omega_p$, the difference-type combination resonance as [14]

$$\Omega_{dr}=-\omega_p+\omega_q\pm\varepsilon\sqrt{-\frac{R_{pq}R_{qp}}{\omega_p\omega_q}-\left(\frac{\mu C_{ii}}{\varepsilon}\right)^2}, \tag{29}$$

where

$$i=p,q.$$

From these equations, it can be easily seen that the sum- and difference-type combination resonance cannot exist simultaneously for any pair of natural frequencies ω_p and ω_q.

While the results such as 'elastic stability boundaries' of the system without damping have been already obtained, the dynamic instability may occur only at the amplitude of the force greater than a certain minimum value in the presence of damping. Furthermore, the critical value of excitation parameter, ε_{cr} for instability can be obtained as,

$$\varepsilon_{cr}=\mu C_{ii}\sqrt{\frac{\omega_p\omega_q}{|R_{pq}R_{qp}|}},$$

where

$$i=\min(p,q).$$

4. Numerical results and discussions

The top and bottom layers of the plate are assumed to be made up of piezoceramic (PZT G1195N), whereas the middle layer is an isotropic material (Aluminum alloy 2024-T4). Table 1 shows the material properties of the model. To check the numerical results, we choose the boundary conditions of the plate are free on all edges as in Ref. [14].

The results are presented for three aspect ratios(λ) equal to 2, 1 and 0.5 with the thickness ratio(γ) equal to 0.01. Also, non-dimensional frequency and load parameters are introduced to present numerical data in the figures:

$$\Omega^2=\frac{\bar{m}\omega^2a^4}{D},\quad Q=\frac{Pa^2}{D}.$$

4.1. Constant load

4.1.1. Eigenvalue curves

Figs. 2(a)–(c) show the eigenvalue curves for the case without damping, that is to say, $G=0$. In the figures, $Q_{F,1}$ and $Q_{F,2}$ denote the flutter loads for $\lambda=2,1$ and 0.5, respectively.

Table 1
Material properties of PZT G1195N and aluminum alloy 2024-T4

		PZT	2024-T4
Young's moduli (GPa)	$E_{11}=E_{22}=E_{33}$	63.0	73.0
Poisson's ratio	$v_{12}=v_{13}=v_{23}$	0.3	0.3
Shear moduli (GPa)	$G_{12}=G_{13}=G_{23}$	24.2	28.1
Density ($kg\,m^{-3}$)	ρ	7600	2800
Piezoelectric constants ($m\,V^{-1}$)	$d_{31}=d_{32}$	2.54e–10	
Electrical permittivity ($F\,m^{-1}$)	$\Xi_{11}=\Xi_{22}$	1.53e–8	
	Ξ_{33}	1.53e–8	

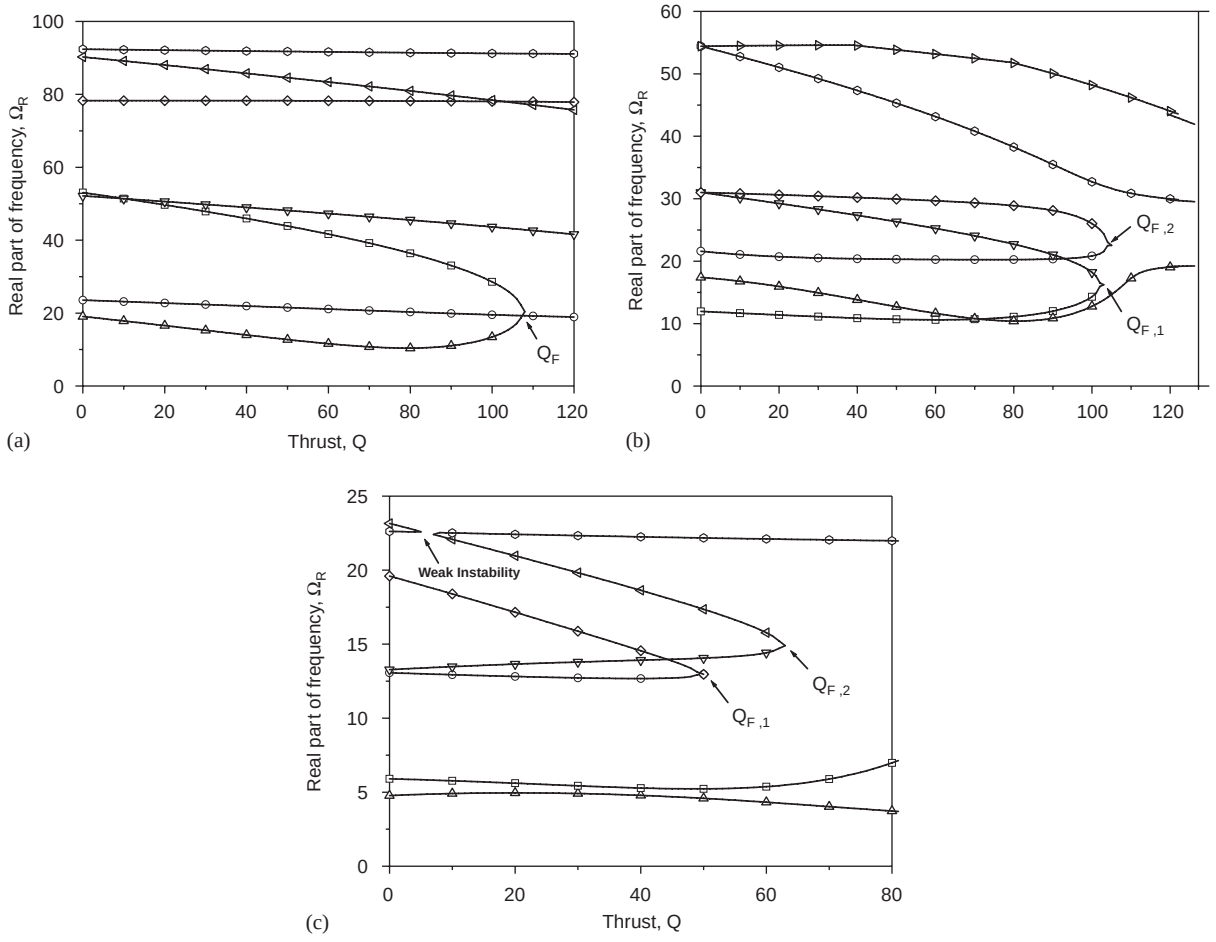

Fig. 2. (a) Eigenvalue curves without damping (λ=2), (b) eigenvalue curves without damping ($\lambda=1$), (c) eigenvalue curves without damping ($\lambda=0.5$).

For $\lambda = 2$, the magnitude of Q_F is about 107.3, and is almost equal to the data in Ref. [14]. For $\lambda = 0.5$, there exists weak instability due to higher modes, and this type of flutter sometimes determines the critical load of structure as in Refs. [11,12].

4.1.2. *Effect of piezoelectric layers*

Damping effect is considered in the piezoelectric layers. Then the frequency are changed to be complex values for all levels of thrust Q. Furthermore, the two curves of the real part of

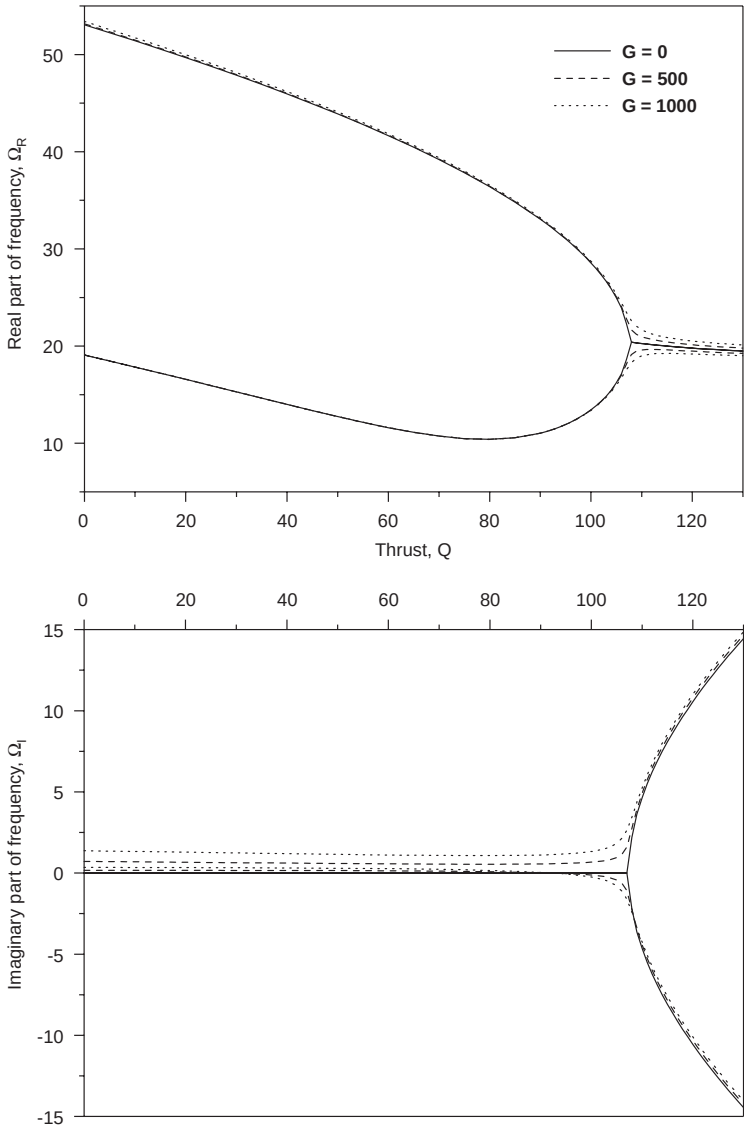

Fig. 3. Complex eigenvalue curves (λ=2).

frequencies do not merge, but asymptotically approach each other. In this case, the flutter should be defined as the imaginary part of frequency changes from positive to negative.

Fig. 3 shows the eigenvalue curves for $\lambda=2$ as the control gains equal to 0, 500 and 1000, respectively. Eigenvalue curves without damping is an asymptotic curve for the curves with damping both in real and imaginary parts. The ratio of the imaginary part to the real part of frequency is called the true damping ratio, and the magnitude of that characterizes the intensity of the flutter instability. Fig. 4 shows the intensity of instability for the same case as Fig. 3, and the ordinate Ω_I/Ω_R is a measure of the intensity of flutter. The figure shows that the system is dynamically unstable if $\Omega_I/\Omega_R<0$. On the contrary, the intensity for $G\neq0$ is much weaker than that for $G=0$.

Figs. 5(a)–(c) show the results that the lowest flutter loads for $G\neq0$ appear at a lower load than at that for $G=0$. Further, the flutter load for $G\neq0$ drops drastically in contrast to the case for $G=0$. But the magnitude of the critical load is insensitive to the change of the non-zero gain G. However, in Fig. 5(c), the intensity of the weak flutter becomes weaker and disappears, or dies out as damping is further increased. It is clear that the damping has a destabilizing effect on structures subjected to the follower force, but stabilizes the weak flutter.

4.2. Load with a pulsating part

4.2.1. Parametric resonances

Without damping, stability transition curves in the ε–Ω_{dr} plane are presented for three aspect ratios λ equal to 2, 1 and 0.5, respectively (Figs. 6(a)–(c)).

As shown in the figures, the instability regions are very sensitive to the aspect ratios. For $\lambda=0.5$, only sum-type combination resonance appears, but for $\lambda=2$, only difference-type exists. However,

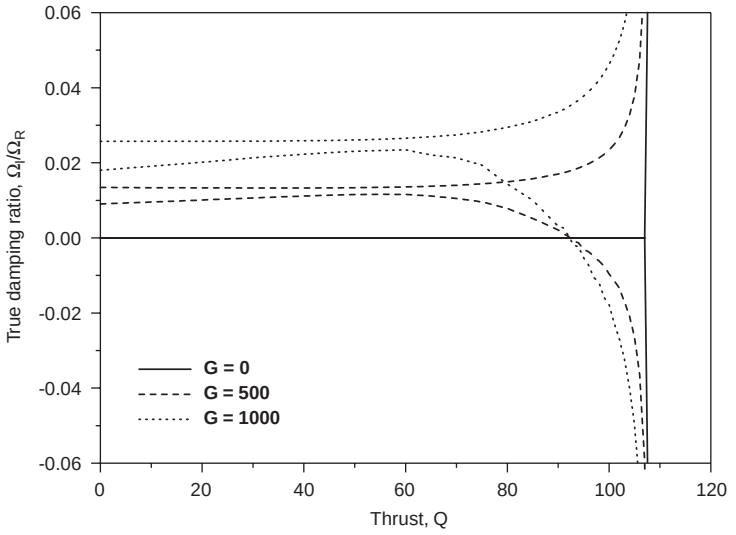

Fig. 4. Intensity of stability ($\lambda=2$).

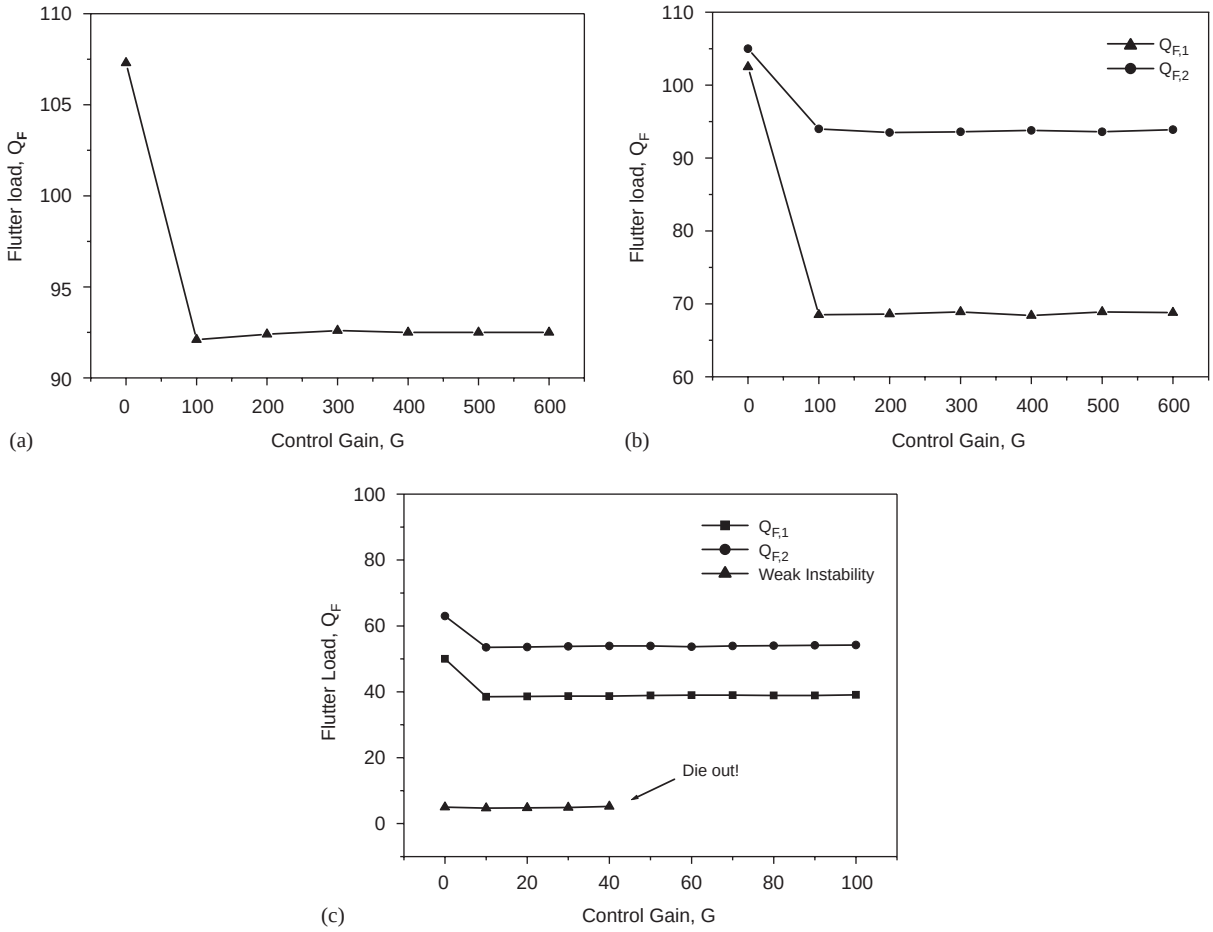

Fig. 5. (a) Flutter load shift ($\lambda = 2$), (b) flutter load shift ($\lambda = 1$), (c) flutter load shift ($\lambda = 0.5$).

for the case of $\lambda = 1$, two types of instability region are observed simultaneously. This is a result of the sign of the geometric stiffness matrices, R_{ij}, R_{ji}. Also the combination resonance of two types, such as symmetrical or non-symmetrical modes, appears selectively. We can see that only two symmetrical (bending) modes are combined with each other, or non-symmetrical (twisting) modes are united each other. Furthermore, the dominant instability regions are observed around $2\omega_1$, $2\omega_2$ regardless of the aspect ratios.

4.2.2. Effect of active damping layer

Fig. 7 shows the change of instability regions when the plate is actively damped by piezoelectric layers.

In this figure, the unstable regions decrease with the proportional to magnitude of G, and shift to the right when the control gain G exists. In other words, the stable region is enlarged when the plate is damped, and active-damping layer shows the stabilizing effect.

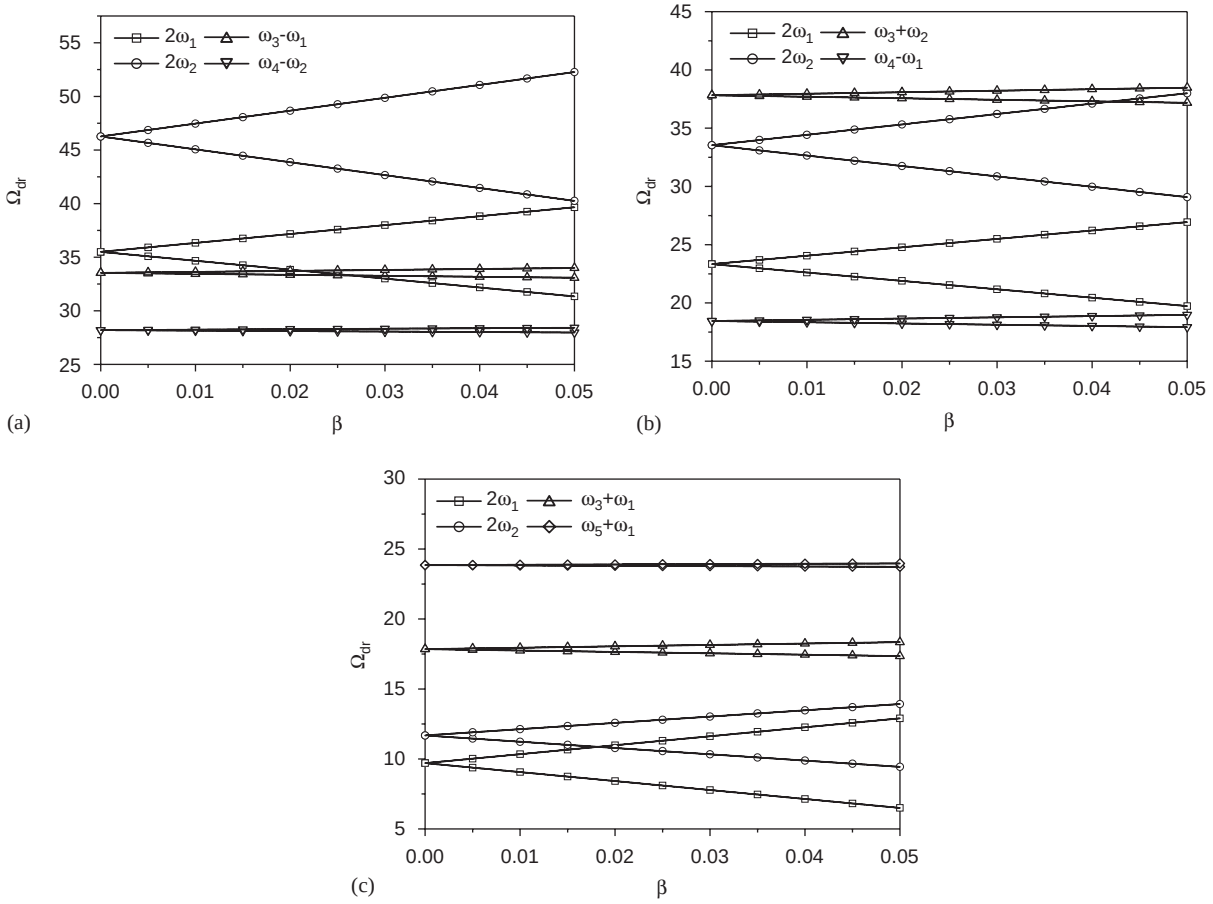

Fig. 6. (a) Parametric instability ($\lambda = 2$), (b) parametric instability ($\lambda = 1$), (c) parametric instability ($\lambda = 0.5$).

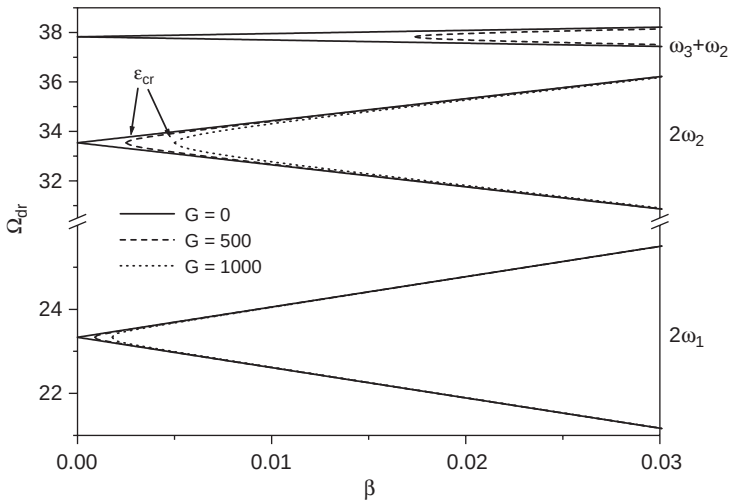

Fig. 7. Parametric instability region in damped system ($\lambda = 1$).

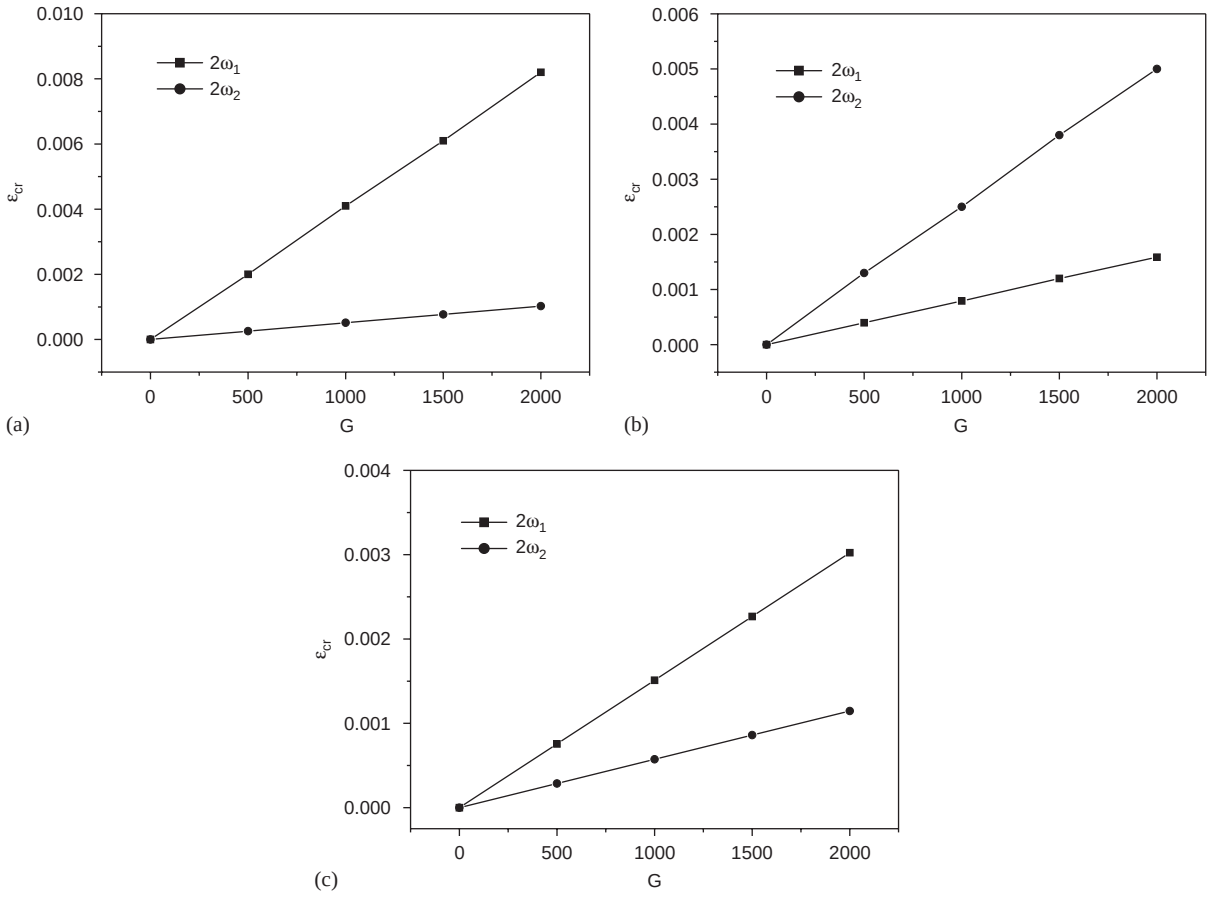

Fig. 8. (a) Critical value of the excitation parameter ($\lambda = 2$), (b) critical value of the excitation parameter ($\lambda = 1$), (c) critical value of the excitation parameter ($\lambda = 0.5$).

To investigate the rate of decrease, we can define the critical value of excitation parameter, ε_{cr} and see the relation between ε_{cr} and G. Figs. 8(a)–(c) suggest that critical value of excitation parameter are almost linearly increased as the control gain is increased. In this figure, we see the main instability region to be main concentrated around $2\omega_1$, $2\omega_2$.

5. Conclusions

In this study, the dynamic stability of plate with the piezo-laminated active-damping layer under a thrust is investigated. As a result, even slight damping was found to bring about considerable change to the dynamic characteristics, and these results can be summarized as follows.

When the plate is subjected to a constant thrust, flutter instability may appear. And eigenvalue curves for the case of $G = 0$ are asymptotic curves of those for the case of $G \neq 0$ both in real and

imaginary parts. Damping effect of piezoelectric layers drastically destabilizes the strong flutter instability, that is, imaginary part of eigenvalue curve for $G \neq 0$ becomes negative at a lower load than that for $G = 0$. But, the flutter load in the system with damping is insensitive to the change in the magnitude of damping effect. However, damping effect stabilizes the weak flutter instability. The intensity of the weak flutter becomes weaker and it dies out as damping is further increased.

Parametrically excited system may produce parametric resonance. The aspect ratio affects the types and width of parametric resonance. And numerical results show that the unstable region decreases in actively damped system. Also, the critical value of excitation parameter that represents width of instability region is linearly proportional to the control gain, G.

References

[1] K.Y. Lam, X.Q. Peng, G.R. Liu, J.N. Reddy, A finite-element model for piezo-electric composite laminates, *Smart Materials and Structures* 6 (1997) 583–591.

[2] G.R. Liu, X.Q. Peng, K.Y. Lam, Vibration control simulation of laminated composite plates with integrated piezoelectrics, *Journal of Sound and Vibration* 220 (1999) 827–846.

[3] C. Saravanan, N. Ganesan, V. Ramamurti, Analysis of active damping in composite laminated cylindrical shells of revolution with skewed PVDF sensors/actuators, *Composite Structures* 48 (2000) 305–318.

[4] V. Balamurugan, S. Narayanan, Shell finite element for smart piezoelectric composite plate/shell structures and its application to the study of active vibration control, *Finite Elements in Analysis and Design* 37 (2001) 713–738.

[5] H.S. Tzou, Y. Bao, V.B. Venkayya, Parametric study of segmented transducers laminated on cylindrical shells, Part 1: sensor patches, *Journal of Sound and Vibration* 197 (1996) 207–224.

[6] H.S. Tzou, Y. Bao, V.B. Venkayya, Parametric study of segmented transducers laminated on cylindrical shells, Part 2: actuator patches, *Journal of Sound and Vibration* 197 (1996) 225–249.

[7] Y. St-Amant, L. Cheng, Simulations and experiments on active vibration control of a plate with integrated piezoceramics, *Thin-Walled Structure* 38 (2000) 105–123.

[8] C. Niezrecki, H.H. Cudney, Creating and verifying a research-grade simply supported cylinder with PZT actuation, *Journal of Sound and Vibration* 228 (1999) 961–975.

[9] W.S. Hwang, H.C. Park, Finite element modeling of piezoelectric sensors and actuators, *AIAA J.* 31 (1993) 931–937.

[10] J.N. Reddy, On laminated composite plates with integrated sensors and actuators, *Engineering Structures* 21 (1999) 568–593.

[11] K. Higuchi, E.H. Dowell, Dynamic stability of a rectangular plate with four free edges subjected to a follower force, *AIAA J.* 28 (1990) 1300–1305.

[12] K. Higuchi, E.H. Dowell, Effects of the poisson ratio and negative thrust on the dynamic stability of a free plate subjected to a follower force, *Journal of Sound and Vibration* 129 (1989) 255–269.

[13] A.H. Nayfeh, D.T. Mook, Parametric excitations of linear systems having many degrees of freedom, *Journal of the Acoustical Society of America* 62 (1977) 289–381.

[14] Y.S. Choo, J.H. Kim, Dynamic stability of rectangular plates subjected to follower forces, *AIAA J.* 38 (2000) 353–361.

[15] T.W. Kim, J.H. Kim, Parametric instability of a cross-ply laminated beam with viscoelastic properties under a periodic force, *Composite Structures* 51 (2001) 205–209.

[16] M.A. Langthjem, Y. Sugiyama, Dynamic stability of columns subjected to follower loads: a survey, *Journal of Sound and Vibration* 238 (2000) 809–851.

[17] I. Svensson, Dynamic instability regions in a damped system, *Journal of Sound and Vibration* 244 (2001) 779–793.
[18] Xin-Mai Yang, Ya-Peng Shen, Dynamic instability of laminated piezoelectric shell, *International Journal of Solids and Structures* 38 (2001) 2291–2303.
[19] Lien-Wen Chen, Chung-Yi Lin, Ching-Cheng Wang, Dynamic stability analysis and control of a composite beam with piezoelectric layers, *Composite Structures* 56 (2002) 97–109.